Influence of the Aspect Ratio of Bioactive Nanofillers on Rheological Behavior of PMMA-Based Orthopedic Materials

Tse-Ying Liu,[1] San-Yuan Chen,[1] Dean-Mo Liu[2]

[1] Department of Materials Science and Engineering, National Chiao-Tung University, 1001 Ta-hsueh Rd., Hsinchu, Taiwan, Republic of China

[2] ApaMatrix Technologies Inc., 58-7151 Moffatt Road, Richmond, British Columbia, Canada V6Y3G9

Received 30 September 2003; revised 17 February 2004; accepted 25 February 2004
Published online 1 June 2004 in Wiley InterScience (www.interscience.wiley.com). DOI: 10.1002/jbm.b.30072

Abstract: In this investigation, calcium-deficient hydroxyapatite (CDHA) nanocrystals with needle-like geometry were synthesized and incorporated with Poly(methyl methacrylate), PMMA, to form CDHA–PMMA nanocomposites. Rheological behaviors of the PMMA–CDHA melting suspensions were systematically investigated in terms of solid loading and aspect ratio of the CDHA nanoparticles. The maximum solid loadings of nano-CDHA particles with aspect ratios of 7.2, 10.4, and 17 were determined to be 28, 31, and 57%, respectively. An increase in solid concentrations causes pronounced shear-thinning behavior. This result suggests that a strong interaction, including Van der Waals attraction and mechanical interlocking, between the nano-CDHA particles makes the nanocomposite mixture more non-Newtonian. Furthermore, it was found that packing efficiency and yield strength in the suspension were strongly influenced by the aspect ratio, especially above the critical value of 8.8. The obtained critical aspect ratio and solid content provide not only appropriate design in the PMMA–CDHA polymeric suspension for fabrication process but also optimal conditions for the fabrication of orthopedic devices via injection molding or extrusion. © 2004 Wiley Periodicals, Inc. J Biomed Mater Res Part B: Appl Biomater 71B: 116–122, 2004

Keywords: rheology; nanoneedle particle; aspect ratio; solid loading; hydroxyapatite; PMMA

INTRODUCTION

Poly(methyl methacrylate), PMMA, has long been widely used as bone cement and on orthopedic devices such as bone screws, pins, etc. The prime advantage of using the PMMA cement is that it is easily conformed to defective surrounds of any geometry. However, clinical practices revealed that the PMMA had several drawbacks such as a weak bone–cement interface[1–4] that renders PMMA prostheses more susceptible to fail after implantation.

Recently, the incorporation of a bioactive reinforcement phase into PMMA offered an advantage to overcome those aforementioned deficiencies, and moreover, improve mechanical integrity with the PMMA.[5–7] Among those reinforcement phases, bioceramic-based materials such as tricalcium phosphate (Ca/P = 1.5) and hydroxyapatite (Ca/P = 1.67) are most widely employed for clinical practices, simply because they exhibit considerably improved biological affinity and activity to surrounding host tissues when implanted.[8–10] Furthermore, both compositions are chemically similar to the mineral constituent of human hard tissue. However, bone mineral (natural biocrystal) has essentially a calcium-deficient apatitic structure with a Ca/P ratio of about 1.5, which is compositionally similar to tricalcium phosphates, $Ca_3(PO_4)_2$, (Ca/P = 1.5) and structurally similar to stoichiometric hydroxyapatite, $Ca_{10}(PO_4)_6(OH)_2$, (Ca/P = 1.67).

It is well known that the natural biocrystals with a needle-like or rod-like shape are well aligned along a specific direction with the polymer matrix, that is, collagen, to form nature bone, which exhibits better mechanical properties compared to individual components and those existing synthetic biomaterials. So far, several studies have been focused on the development of nanocomposites to simulate nature bone in an apatite structure.[11–15] For example, Adriana et al. developed a biomimetic process to control the alignment of nanoparticles in the nanocomposites.[11] However, these methods could not be applied for the fabrication of medical devices with a complex shape. On the other hand, a stress-induced process such as injection-molding or extrusion can be used for the alignment of nanoparticles in polymeric suspension under a high shear rate. Although some investigations have

Correspondence to: S.-Y. Chen (e-mail: sychen@cc.nctu.edu.tw)
Contract grant sponsor: the National Science Council of the Republic of China; contract grant number: NSC-92-2216-E-009-025

been focused on the relationship between rheological behavior and nanoparticle structure of polymeric suspension in the nanocomposite mixtures,[16–18] little information is available on the rheological properties of PMMA-HA nanocomposite with different aspect ratios of the nanoparticles for the fabrication of orthopedic parts like bone fixation devices.

Although Ti or C fibers can be incorporated into the PMMA to enhance the mechanical properties, it is more desirable if nanometric calcium-deficient apatite crystals (hereafter termed CDHA) with a pertinent aspect ratio, mimicking that of the mineral constitute in a natural bone structure, can be introduced in the PMMA matrix. The improvement in both the biological affinity and mechanical properties of the resulting PMMA–CDHA composites is then expected. Therefore, nanometric needle-like CDHA crystals, instead of Ti or C fibers, were synthesized and employed in this work to study the role of the aspect ratio of CDHA nanoneedle crystals in the rheological behavior of the PMMA–CDHA mixture. As a first part of the whole project, understanding of the rheological behavior of the PMMA–CDHA blend in this study should provide fundamental and valuable processing information in terms of solid content and aspect ratio of the reinforced phase as reported in this communication, for the fabrication of PMMA-based orthopedic devices by injection molding or an alternative thermal molding process.

MATERIALS AND METHODS

Synthesis of CDHA Nanoparticle

The calcium-deficient hydroxyapatite (CDHA) nanoparticles with a Ca/P molar ratio of 1.5 were fabricated by the coprecipitation method with $Ca(CH_3COO)_2$ and H_3PO_4 as Ca and P precursors, respectively. Prior to coprecipitation reaction, the pH value of H_3PO_4 solutions were kept above 12 by using the NaOH solution. Subsequently, 0.001 wt % poly(acrylic acid) (PAA) (Aldrich Chemical, MW 2000) was added into the alkalized H_3PO_4 solutions. To control the CDHA particle with different aspect ratios, three different adding rates of 5 mL/min, 30 mL/min, and 55 mL/min were used to drop $Ca(CH_3COO)_2$ aqueous solution (0.5 *M*) into H_3PO_4 solution (controlled at 0.33 *M*) at 60 °C.[19] During the titration process, the temperature deviation of each mixture was monitored and kept less than 3 °C. After filtration and washing by acetone for several times, the precipitate dough was then mixed in 80 mL acetone to form three kinds of CDHA suspensions. The solid content in each CDHA–acetone suspension was determined by measuring the weight difference between before and after the removal of the diluting medium at 105 °C.

CDHA–PMMA Composite Mixtures

Various volume from 5 to 15% CDHA nanoparticles with different aspect ratios (AR = length of particle/width of particle) were dispersed in the PMMA–Acetone (PMMA: Aldrich Chemical Corp. MW 13,000) polymer solution to form a PMMA–CDHA composite. After stirring for 24 h, the CDHA–PMMA suspensions were dried to remove the diluting solvent and then subjected to heat treatment in vacuum oven for the removal of the residual solvent. After that, the CDHA–PMMA nanocomposite powders can be obtained after pulverization.

Rheometrical Measurement

The rheological behavior of the mixtures with different concentrations of CDHA nanoparticles was examined at a working temperature of 240 °C using capillary rheometry (Schimadzu, CFT-500D). The specimens were first prepared into a cylindrical shape of 10 × 10-mm dimensions via a uniaxial molding at a compressive pressure of 30 MPa at 160 °C. The cylindrical specimen was then placed into the cavity die of the capillary rheometer. The capillary die has a size of 1 mm in diameter, located at the bottom of the cavity. After the sample was stabilized at the testing temperature of 240 °C for several minutes, the specimen was compressed with a predetermined uniaxial pressure.

To eliminate the entrance and end effect of the rheological data, both the first and final 1-mm region of the 10 mm-height specimens were excluded. In addition, the Rabinowitsch equation was also adopted for shear rate correlation due to wall effect. The relationship between shear stress (τ) and pressure drop along the specimen dimension can be determined with the use of Bagley model, as follows:[20]

$$\tau = \frac{PR}{4L} \tag{1}$$

where P, R, and L represent the values of pressure drop, capillary radius, and capillary length, respectively. The shear rate (γ) was determined by converting the ratio of the volume flow rate (F) to the capillary radius (R) through,

$$\gamma = \frac{4F}{\pi R^3} \tag{2}$$

The shear viscosity (η) was then determined by;

$$\eta = \frac{\tau}{\gamma} \tag{3}$$

Generally, three runs were conducted for each composition and aspect ratio to ensure the accuracy and the reproducibility of the rheological data. If needed, five runs were performed for more accurate results.

RESULTS AND DISCUSSION

Flow Behavior

The XRD patterns in Figure 1 show that the synthetic powders can be indexed as a calcium-deficient HA (CDHA) phase irrespectively of the addition rate. According to TEM obser-

vation, the morphology of the precipitate crystals exhibits needle-like geometry with different aspect ratios (L/d, length/diameter), ranging from 7.2, 10.4, to 17 for the addition rate of 5, 30, and 55 mL/min, respectively. (TEM photographs were not shown here.)

The flow behavior of the PMMA–CDHA mixtures can be characterized by a shear rate (γ)-viscosity (η) curve (derived simply from $\eta = K\gamma^{n-1}$), as shown in a log–log plot of Figure 2(a–c) for CDHA nanoneedles with AR = 7.2, 10.4, and 17, respectively. It is evident that the mixtures are a shear-thinning character and the flow behavior of the mixtures is as a function of both AR and concentration of the nanoneedles. The flow index n is generally falling in the range between 0.4 and 0.5 for the mixtures with 5 and 10% concentration of nanoneedles. Even increasing CDHA concentration up to 15%, the difference in the flow index for the composition with the smallest AR [Figure 2(a)] is essentially much less pronounced over the range of the solid concentration employed. This may indicate that the flow behavior as well as the suspension structure of the mixtures prepared with the nanoneedles of the smallest AR is similar. Accordingly, this could be true for the nanoparticles with a lower AR below a certain solid loading where the interparticle interaction, including surface attraction or mechanical interlocking, may remain similar in magnitude.

On the other hand, for the compositions with larger AR, a smaller n value was observed at a 15% solid loading as revealed from Figure 2(b,c). While comparing to Figure 2(a), a considerable reduction in the flow index (n), appearing at 15% loading, may suggest that the nanoparticles with a higher AR should exert strong influence onto suspension structure and flow behavior. From those measured data in Figures 2(b,c) for high-AR particles, it seems to indicate that at lower solid loadings, that is, 5 and 10%, the interactions between the nanoneedles should be not as significantly strong as that at 15%.

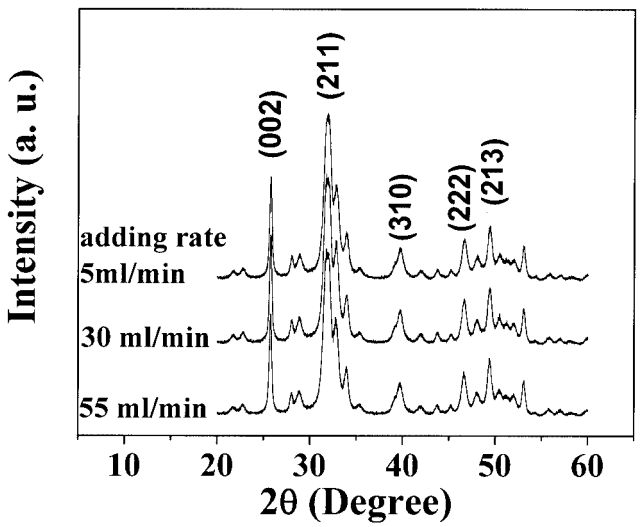

Figure 1. X-ray diffraction patterns of the calcium phosphate powders prepared with various addition rates.

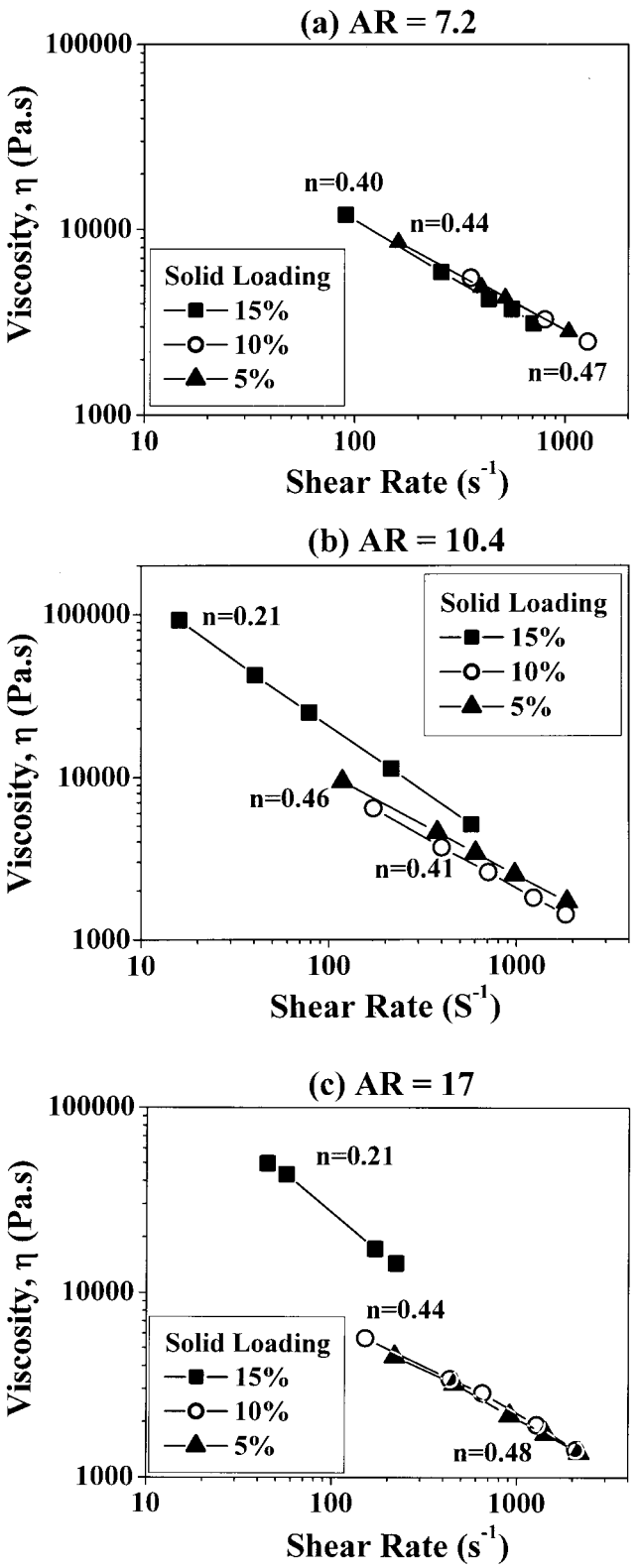

Figure 2. Shear rate–shear viscosity relationship for CDHA–PMMA mixtures with nanoneedles of different aspect ratios.

However, a particle network structure with more extensive entanglement with random distribution of the nanoneedles should arise because of increasing solid loadings, that is, 15%

in the current system. If this assumption in structural development is correct, then, we can speculate that the mixtures with solid loading as high as 15% may have an open network structure with voids between the closely connect framework filled with polymer melt. With such an interconnect structure, the flowability of the polymer melt was then effectively retarded and a higher shear viscosity can be expected under an identical shear rate (or shear stress), leading to a higher shear-dependent character than that at lower solid concentrations.

Yield Strength

With the use of the Casson's model,[21] eq. (4), the yield strength of the mixtures can be obtained by extrapolating the straight lines obtained from the $\tau^{1/2} - \gamma^{1/2}$ plot to zero shear rate.

$$\tau^{1/2} = \tau_y^{1/2} + c\gamma^{1/2} \tag{4}$$

where τ_y is the yield strength.

Figure 3 shows Casson's correlation for the mixtures with AR = 17, where straight lines for each solid loading can be obtained in Casson's plot. After extrapolating to zero shear rate, the τ_y was calculated, and is also illustrated in the figure. It is observed that τ_y first increases slightly with increasing solid loading from 5 to 10%, but considerably increased at 15% loadings. Similar behavior is also observed for other mixtures, as illustrated in Figure 4. However, as expected, the τ_y at lower solid loadings, that is, <10%, does not show much difference for each category of AR, but the difference becomes more pronounced when the solid concentration is increased up to 15%.

The yield strength is merely a direct indication of the strength of the particle network within the matrix, which has

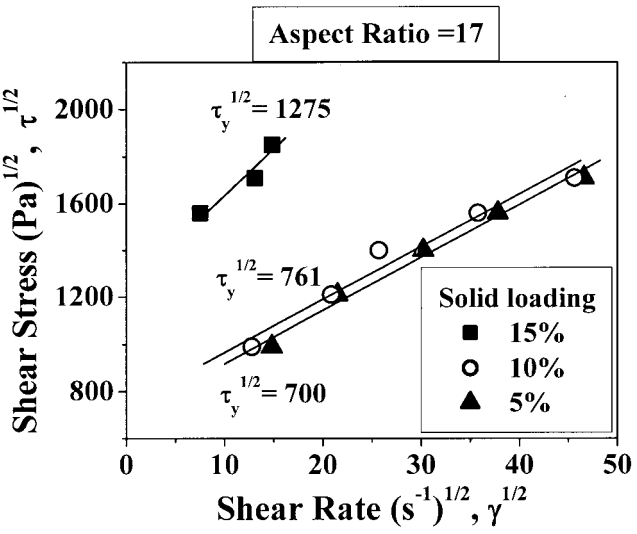

Figure 3. Casson's correlation for the mixtures with AR = 17, corresponding yield stress can be obtained by extrapolating the straight line at zero shear rate.

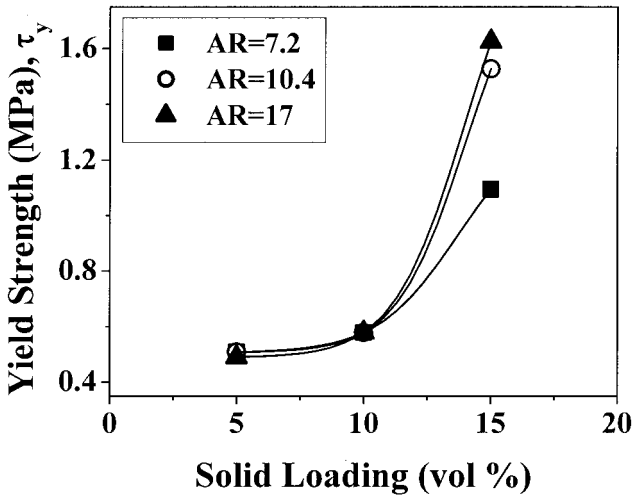

Figure 4. Yield stress of the CDHA–PMMA mixtures increases with solid concentration, and a considerable increase in the yield stress was observed for CDHA of a higher aspect ratio.

been well recognized due to net attractive interaction. For high-aspect ratio particles, mechanical interlocking between neighboring particles should play some role. In a previous investigation,[22] Liu experimentally verified that the yield strength is correlated linearly with the Van der Waals potential between two identical spheres; however, the near-surface potential should remain identical for particles with various geometries. Furthermore, it turns out to be more pronounced for smaller particles because the particle-to-particle separation (λ) is getting smaller for nanometric dimension by:[22]

$$\lambda = \frac{4}{3} r \frac{\Phi_m - \Phi}{\Phi} \tag{5}$$

where Φ_m is the maximum solid loading of a given mixture system, r is the particle radius, and Φ is the solid faction of the mixture. For particles with a high aspect ratio such as needlelike geometry, eq. (5) may be suitable only when the needle-like particles are well aligned with parallel configuration, and λ_{rod} obtained from eq. (5) is approximated as the needle-to-needle distance, as schematically illustrated in Figure 5. λ is proportional to the particle radius (r) and the decreased solid fraction (Φ). The resulting Van der Waals potential is increased proportionally with both decreased r of the particles and increased solid fraction of the mixture. Therefore, an enhanced yield strength is expected.

However, real network structure in the mixtures, when first prepared, is far from being idealized and simplified as depicted in Figure 5, but randomly oriented. This gives complexity upon a quantitative analysis due to the increase in the randomness and geometry of the dispersed particles. One of the most commonly seen phenomena is a direct physical contact of the needle-like particles spreading over the entire mixture volume. Once it happens, mechanical interlocking with enhanced friction, except the attractive potential, between needles is thus reasonably expected. If this occurs, then

the mechanical friction force should increase because of more "contact points" due to the introduction of higher fractions and/or higher aspect ratio of the nanoneedles.

Further analysis of the frictional force could be feasible but not the primary focus of this article. Therefore, the variation of suspension structure in terms of particle packing efficiency seems able to provide clues for better understanding on rheological behaviors. It is conceivable that the interparticle friction, stemming from the physical "contact" of the needles in this communication, should directly affect the efficiency of particle packing. This means that a maximum solid fraction (Φ_m) should be achievable and inversely proportional to the density of the contact points. Because only when particles are physically separated from each other in the mixture suspension, effective volume in the suspension for further deformation is available, permitting a higher maximum loading to be attained. However, while particles are closely packed with each other by physical contact, the effective space is then diminished, and no deformation can be detected, restricting the development toward higher level of Φ_m.

Therefore, the estimation of the maximum loading in a given mixture is able to provide physically meaningful evidence for better understanding the interlocking effect in this nanocomposite system. To estimate the maximum fraction, Liu[23] recently proposed a simple two-parameter model that is useful to predict Φ_m for a number of suspension systems with precision. Here, we employ the model, having an analytical form:

$$1 - \eta^{-1/2} = a\Phi + b \tag{6}$$

where Φ_m can be determined via the slope (a) and intercept (b) in $(1 - \eta^{-1/2}) - \Phi$ plot by:

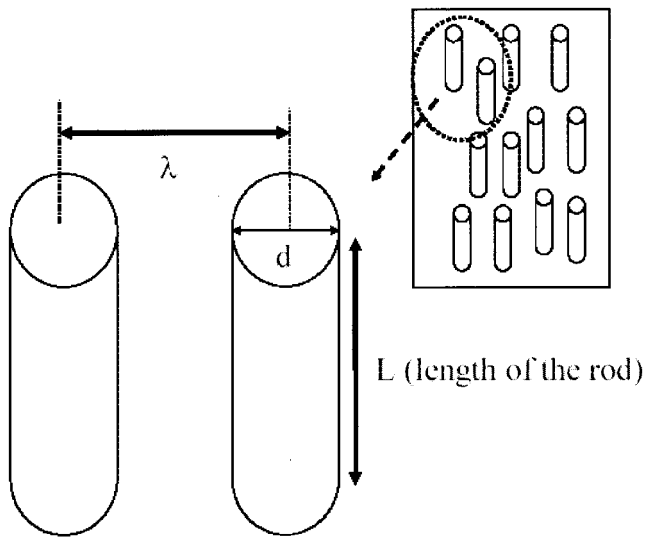

Figure 5. Dimensional configuration between two nanoneedles with an interparticle distance of λ. Upper right is a schematic drawing of a given volume of the nanoneedle mixture.

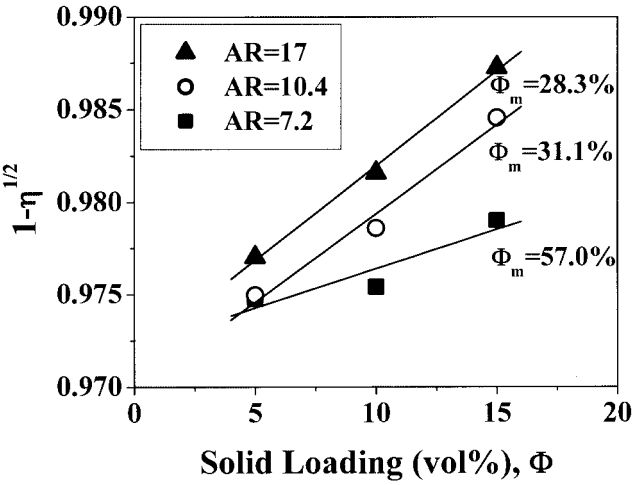

Figure 6. Maximum solid load (Φ_m) of the CDHA–PMMA mixtures under investigation can be determined via an extrapolation of the linear $(1 - \eta^{-1/2}) - \Phi$ correlation at $1 - \eta^{-1/2} = 1$. A corresponding AR value of the mixtures is also indicated.

$$\Phi_m = \frac{1 - b}{a} \tag{7}$$

As expected, Figure 6 shows a linear relationship according to eq. (6), but surprisingly, the correlation is well suitable for high-aspect ratio nanoparticles, although it was originally derived from sphere model.

The Φ_m obtained is also described in Figure 6 for nanoparticles with different aspect ratios. It is evidenced that an increase in the aspect ratio causes a decrease in packing efficiency, resulting in a lower Φ_m. This further substantiates that the packing efficiency of the nanoneedles is considerably retarded with the increased aspect ratio. In other words, for high-aspect ratio nanoparticles, percolation of the particle can be easily reached with lower solid fraction than that of particles with low aspect ratio. Based on this argument, it is reasonable to believe that as aforementioned, a huge number of physical contacts between nanoneedles do give considerable yield strength to the mixtures, and accordingly, mechanical interlocking associated with the rising effect of frictional force is largely expected.

Aspect Ratio-Dependent Suspension Property

By plotting the Φ_m in terms of AR (symbolized as ξ), Figure 7 shows dependence of maximum solid concentration on the aspect ratio of the CDHA particles, where an extra point (arrow indicated) was derived from sphere suspension (AR = 1). A sigmodal behavior (solid line) was clearly observed. Although the data point at AR = 1 is borrowed from other well-characterized systems,[23] it is generally believed that a randomly close packing of spherical particles with a relative packing density of ~0.64 can be attainable under infinite shear. A steeper transition in the sigmodal curve can be found with the aspect ratio (ξ) in the range between 7.2 and 10.4. This is suggestive of an existing critical aspect ratio (ξ_c),

above which the suspension structure may be considerably altered because of poorer packing efficiency. To determine the ξ_c, a simple third-order polynomial equation in eq. (8) was employed for curve fitting (dash curve in Figure 7). Although the curve-fitting is not matched very well with the experimental data, the fitted curve still shows good consistence with the data in the important aspect ratio (ξ) range of 7.2 to 10.4. Therefore, the transition point can be further derived by double differentiating eq. (8) in terms of ξ, and a value of 8.8 was calculated while solving the differentiated form of eq. (8) at $d^2\Phi m/d\xi^2 = 0$.

$$\Phi_m = 0.0952\,\xi^3 - 2.512\,\xi^2 + 13.753\,\xi + 52.664 \qquad (8)$$

This value at $\xi_c = 8.8$ seems in agreement with a preceding observation of the Φ_m determined in Figure 6, suggesting that the resulting particle packing efficiency is substantially retarded when the used nanoneedles have an aspect ratio greater than 8.8 in the current system. Furthermore, this phenomenon becomes more pronounced when the solid loading reaches (and goes above) 15%. The poorer particle packing efficiency due to the influence of the particle aspect ratio is then believed because of the increased density of physical contacts between the nanoneedles. It can be then reasonably expected for a significant increase in the frictional force among the contact nanoneedles. As further evidenced from a correlation between the aspect ratio and yield strength, as shown in Figure 8, where a considerable increase in the yield strength can be found when the particle aspect ratio is increased from 7.2 to 10.4 for 15% of the solid loading.

Therefore, it is clear that above a certain solid loading, the aspect ratio of the particles turns into a dominant factor on the variation of suspension structure and corresponding yield

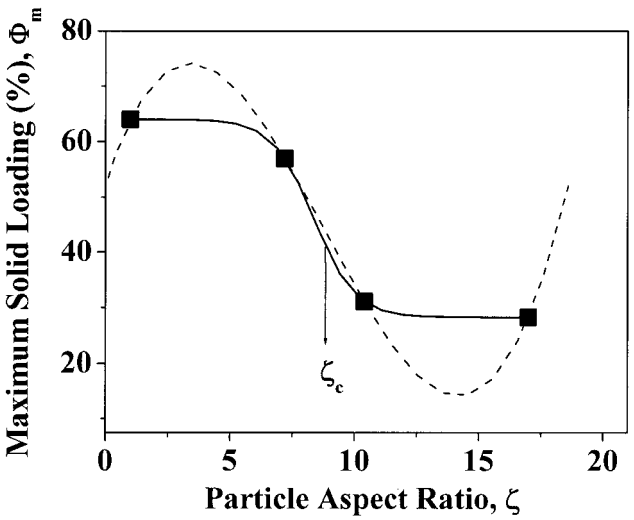

Figure 7. Dependence of maximum solid concentration on the aspect ratio of the CDHA particles, where a sigmodal behavior was clearly observed. A simple third-order polynomial Equation was employed for curving fitting (dash curve), which facilitates estimation of the deflection point, that is, critical aspect ratio, ξ_c, in the sigmodal correlation.

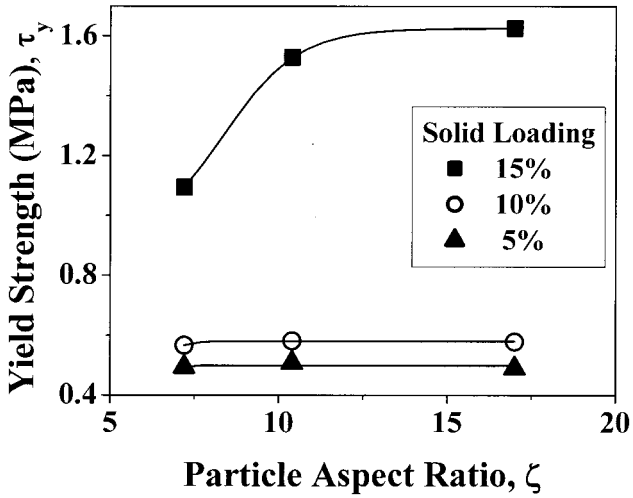

Figure 8. The variation of the yield strength of the CDHA–PMMA mixtures as a function of particle aspect ratio at different solid loads, where the influence of particle dimension becomes more pronounced only when solid load reaches 15%.

behavior. It is more interesting to note that the critical aspect ratio, for the first time so far as we know, in the current mixture can be semiempirically determined via a simple mathematic treatment.

In this work, the use of capillary rheometry instead of dynamic rheometry for the characterization of the rheological properties of the PMMA–CDHA blends does provide more realistic flowing behavior of the melting suspension under the operation of injection molding or thermal extrusion process. The influence of the nanometric CDHA crystals on the rheological behaviors of the blend allows the nano-sized CDHA particles dispersed in the nanocomposites to be optimized in terms of aspect ratio and loading of the nano-CDHA under sufficient shear rate. However, the effect of the stress-induced alignment of the nano-sized CDHA particles on the mechanical properties of the resulting composite will be reported separately.

CONCLUDING REMARKS

Calcium-deficient hydroxyapatite nanoneedles with different aspect ratios were prepared and incorporated into poly(methyl methacrylate) to form nanocomposite mixtures. The rheological properties and suspension structure of the mixtures were characterized with respect to the particle aspect ratio. Some conclusions can be summarized as follows.

1. The influence of the particle aspect ratio on packing efficiency is significant, and a critical value of the aspect ratio was determined to be 8.8.
2. With increasing the aspect ratio, especially above the critical value, the nanoneedles result in an extensive contact between the particles upon which a poorer packing

efficiency, higher yield strength, and poorer flowability of the mixture suspension can be observed.

3. The maximum solid loadings of nano-CDHA particles with aspect ratios of 7.2, 10.4, and 17 were determined to be 28, 31, and 57%, respectively.
4. Rheological behavior of the PMMA–CDHA mixture as functions of solid loading and aspect ratios of the CDHA nanoparticles provides not only optimal design of nanoparticles in the polymeric suspension but also optimized conditions for the fabrication of PMMA–CDHA-based orthopedic devices.

Thanks are given to ApaMatrix Technologies Inc., Canada, for technical support.

REFERENCES

1. Amstutz HC, Gruen T. Clinical application of polymethylmethacrylate for total joint replacement. In: Ahstrom JP, editor. Current practice of orthopaedic surgery. St. Louis, MO: CV Mosby Company; 1973. p 158–182.
2. Vasquez B, Elvira C, Levenfeld B. Application of tertiary amines with reduced toxicity to the curing process of acrylic bone cements. J Biomed Mater Res 1997;34:129–136.
3. Oonishi H. Mechanical and chemical bonding of artificial joints. Clin Mater 1990;5:217–233.
4. Downes S. Methods of improving drug release from poly-(methyl methacrylate) bone cement. Clin Mater 1991;7:227–231.
5. Vallo CI, Montemartini MA, Fanorich MA, Porto Lopez JM, Candrado TR. Polymethylmethacrylate based bone cement modified with hydroxyapatite. J Biomed Mater Res 1999;48: 174–178.
6. Sogal A, Hulbert SF. Mechanical properties of a composite bone cement; Polymethylmethacrylate and hydroxyapatite. Bioceramics 1992;5:213–224.
7. Dalby MJ, DiSivio L, Harper EJ, Bonefield W. Increasing hydroxyapatite incorporation into poly(methyl methacrylate) cement increases osteoblast adhesion and responses. Biomaterials 2002;23:569–576.
8. Hench LL, Wilson J. Surface-active biomaterials. Science 1984; 226:630–636.
9. Heisa U, Osborn JF, Dune F. Hydroxyapatite ceramic as a bone substitute. Int Orthop 1990;14:329–338.
10. Nanes CR, Simske SJ, Sachdeva R, Wolford LM. Long-term growth and apposition of porous hydroxyapatite implants. J Biomed Mater Res 1997;36:560–563.
11. Bigi A, Boanini E, Panzavolta S, Roveri N. Biomimetic Growth of hydroxyapatite on gelatin films doped with sodium polyacrylate. Biomacromolecules 2000;1:752–756.
12. Bigi A, Boanini E, Panzavolta S, Roveri N, Rubini K. Bonelike apatite growth on hydroxyapatite–gelatin sponges from simulated body fluid. J Biomed Mater Res 2002;59:709–714.
13. Chang MC, Ko C-C, Douglas WH. Preparation of hydroxyapatite–gelatin nanocomposite. Biomaterials 2003;24:2853–2862.
14. Wang X, Li Y, Wei J, de Groot K. Development of biomimetic nano-hydroxyapatite/poly(hexamethtlene adipamide) composites. Biomaterials 2002;23:4787–4791.
15. Itoh S, Kikuchi M, Koyama Y, Takakuda K, Shinomiya K, Tanaka J. Development of an artificial vertebral body using a novel biomaterials hydroxyapatite/collagen composite. Biomaterials 2002;23:3919–3926.
16. Joseph R, McGregor WJ, Martyn MT, Tammer KE, Coates PD. Effect of hydroxyapatite morphology/surface area on the rheology and processability of hydroxyapatite filled polyethylene composites. Biomaterials 2002;23:4295–4302.
17. Bercea M, Navard P. Shear dynamics of aqueous suspensions of cellulose whiskers. Macromolecules 2000;33:6011–6016.
18. Yuan J, Murry HH. The importance of crystal morphology on the viscosity of concentrated suspensions of kaolins. Appl Clay Sci 1997;12:209–219.
19. Bouyer E, Gitzhofer F, Boulos MI. Morphological study of hydroxyapatite nanocrystal suspension. J Mater Sci Mater Med 2000;8:523–531.
20. Bagley EB. End correlations in capillary flow of polyethylene. J Appl Phys 1958;28:624–627.
21. Casson N. A flow equation for pigment oil suspensions of the printing types. In: Mill CC, editor. Rheology of disperse systems. London: Pergamon Press; 1959. p 84–104.
22. Liu DM. Control of yield stress in low-temperature ceramic injection moldings. Ceram Int 1999;25:587–592.
23. Liu DM. Particle packing and rheological property of highly-concentrated ceramic suspensions: Fm determination and viscosity prediction. J Mater Sci 2000;35:5503–5507.